8 SCIENTIFIC HIGHLIGHT OF THE MONTH

Strength, magnetism and stability of metals and intermetallics at extreme loading conditions

Mojmír Šob,[1] Martin Friák,[1,2] Dominik Legut,[1,3] and Václav Vitek[4]
[1]*Institute of Physics of Materials, Academy of Sciences of the Czech Republic, Žižkova 22, CZ-616 62 Brno, Czech Republic,* mojmir@ipm.cz
[2]*Institute of Condensed Matter Physics, Faculty of Science, Masaryk University, Kotlářská 2, CZ-611 37 Brno, Czech Republic,* mafri@ipm.cz
[3]*Department of Chemistry of Materials, Faculty of Chemistry, Brno University of Technology, Purkyňova 118, CZ-612 00 Brno, Czech Republic,* legut@ipm.cz
[4]*Department of Materials Science and Engineering, University of Pennsylvania, 3231 Walnut St., Philadelphia, PA 19104-6272, U.S.A.,* vitek@sol1.lrsm.upenn.edu

Abstract

Theoretical strength, magnetism, stability, and phase transformations in iron and the intermetallic compound Ni_3Al are studied via first-principles electronic structure calculations. Total energies are calculated as functions of parameters characterizing the tetragonal and trigonal transformation paths at various atomic volumes using the spin-polarized full-potential linearized augmented plane waves (FLAPW) method with the generalized-gradient approximation (GGA) for the exchange-correlation energy. The results are displayed in terms of contour plots of the dependence of the energy on parameters of the tetragonal or trigonal deformation and volume. Borders between various magnetic phases are shown. Whereas during tetragonal deformation, iron transforms to antiferromagnetic states, it mostly keeps its ferromagnetic ordering during trigonal deformation. The total energy difference between non-magnetic and ferromagnetic Ni_3Al in the $L1_2$ structure is very small, about 21 meV/formula unit and, therefore, magnetism does not play an important role in stabilization of the $L1_2$ structure. For iron, we discuss the results of simulated tensile tests for uniaxial loading along the [001] and [111] directions as well as for isotropic triaxial tension and compare corresponding tensile strengths. Marked anisotropy of theoretical tensile strength in [001] and [111] direction is elucidated in terms of the presence of higher-symmetry structures along the deformation paths. A table summarizing the values of theoretical tensile strengths calculated up to now is presented.

1. Introduction

The strength of materials is usually controlled by nucleation and motion of dislocations or microcracks. If such defects were not present, the material loaded in tension would only fail if the theoretical, or ideal tensile strength were reached. The stress at which this is achieved is comparable with the Young modulus of the material and it is an upper limit of stresses attainable prior to failure. Until recently loads of this magnitude were approached in studies of the mechanical behaviour of whiskers of very pure metals and semiconductors [1–5]. However, the ideal strength appears to control both the onset of fracture and dislocation nucleation in defect-free thin films and, in particular, in nano-structured materials that are currently being developed. This has been confirmed most eloquently by nanoindentation experiments (see e. g. [6–10]) which suggest that the onset of yielding at the nanoscale is controlled by homogeneous nucleation of dislocations in the small volume under the nanoindenter where stresses approach the theoretical strength. This volume is practically always dislocation free since in well-annealed samples the average dislocation spacing is about 1 μm, while the contact area as well as the depth in which large stresses are attained are of the order of 100 nm.

Theoretically, the ideal strength was studied in the past using semiempirical approaches when describing atomic interactions (for a review see e.g. [11] and the references therein; ideal shear strengths calculated for all basic cubic structures may be found in [12]). However, within such schemes parameters characterizing interatomic forces are fitted to equilibrium properties of the material studied and their transferability to the state when this material is loaded close to its theoretical strength is not warranted. In contrast, ab initio electronic structure (ES) calculations can be performed reliably for variously strained structures and are thus capable to determine the ideal strength of materials without resort to doubtful extrapolations. Nevertheless, most of the ES calculations were directed towards finding the equilibrium state of a given material that corresponds to the minimum of the total energy or towards analysis of relatively small deviations from that state. On the other hand, theoretical strength is related to the maximum force that may be applied to the material without perturbing its stability. It is usually connected with an inflexion point on the dependence of the total energy on deformation parameters.

The first paper dealing with the ideal tensile strength from the first principles was probably that of Esposito et al. [13]. However, those authors have not performed relaxations of dimensions of the loaded crystal in the directions perpendicular to the loading axis. Paxton et al. [14] and Xu and Moriarty [15] calculated shear strength for unrelaxed shear deformation. Other ab initio calculations of properties of the systems far from equilibrium have also been made, such as exploration of the structural stability, but the results were not employed to evaluate the strength [16–20].

Probably the first ab initio simulation of a tensile test, including the relaxation in perpendicular directions to the loading axis, was performed by Price et al. [21] for uniaxial loading along the [001] axis in TiC. Later, our group at the Institute of Physics of Materials in Brno initiated systematic ab initio studies of theoretical strength and stability in metals and intermetallics under extreme loading conditions. In [22], we obtained the theoretical tensile strengths for [001] and [111] loading directions in tungsten. The results compared very well with experiments performed on tungsten whiskers by Mikhailovskii et al. [23]. Further, we calculated ideal tensile strength

in NiAl [24, 25] and Cu [25]. These results found a very good response in the international solid state physics and materials science communities and established a basis for further calculations of ideal tensile strength. Li and Wang [26] computed the ideal tensile strength in Al. Kitagawa and Ogata [27, 28] studied the tensile strength of Al and AlN, but have not included Poisson contraction. The group at the University of California at Berkeley calculated ideal shear strength in Al and Cu [29, 30] as well as in W [31, 32], performed a thorough theoretical analysis of the problem of strength and elastic stability [33] and, among others, verified our values of ideal tensile strength for tungsten [32].

Further calculations of theoretical tensile strength were performed for β-SiC [34], diamond [35, 36], Si and Ge [36], Mo and Nb [37], and for Si_3N_4 [38-40]. Ideal shear strength was recently calculated for TiC, TiN and HfC [41], Si [42] and newly for Al and Cu [43]. Some calculations have been done for nanowires (amorphous Si [44], MoSe nanowires [45]), grain boundaries [46, 47], and interfaces [48].

From 1997, ab initio calculations of theoretical strength under isotropic triaxial (hydrostatic) tension (i.e., negative hydrostatic pressure) also appeared [49–54]. As the symmetry of the structure does not change during this deformation, simpler ab initio approaches may be applied.

Very recently, we have simulated a tensile test in prospective high-temperature materials, namely in transition metal disilicides $MoSi_2$ and WSi_2 with the $C11_b$ structure. This study included calculation of the tensile strength for [001] loading and analysis of bonds and their changes during the test [55, 56]. Theoretical tensile strength of iron in the loading direction [001] was determined in Refs. [57] and [58]; in [59], we compared those results to each other and calculated the tensile strength of iron for uniaxial loading in the [111] direction. Tables summarizing ab initio values of theoretical tensile strengths for various materials are given in Refs. [59-62] and, most up-to date, in Table 1 in Section 6 of the present work. Ref. [61] includes also ab initio values of shear strengths and some semiempirical results. An extensive review of the semiempirical and ab initio calculated values of uniaxial and isotropic triaxial tensile strengths as well as of shear strengths calculated up to 1999 can be found in Ref. [63].

There are more general problems of stability of materials and of phase transformations that are closely related to the tensile tests described above. Namely, the tensile test may be considered as a special case of the so-called displacive phase transformation path [16, 18]. These paths are well known in studies of martensitic transformations. Such transformations play a major role in the theory of phase transitions. They proceed by means of cooperative displacements of atoms away from their lattice sites that alter crystal symmetry without changing the atomic order or composition. A microscopic understanding of the mechanisms of these transformations is vital since they occur prominently in many materials.

Displacive phase transformations are also of interest in studies of epitaxial thin films. Pseudomorphic epitaxy of a cubic or tetragonal (001) film typically results in a strained tetragonal structure. In this case, there is a stress in the (001) plane keeping the structure of the film and of the substrate coherent, and the stress perpendicular to this plane vanishes. A tetragonal phase arises that may be stable or metastable [20]. Similarly, an epitaxial film grown on the (111) plane of a cubic substrate exhibits a trigonal deformation of its lattice, which may be considered as a uniaxial deformation along the [111] axis. In this context it is interesting to

consider the trigonal deformation path, which comprises the bcc, fcc and simple cubic structures as special cases [64-66, 18]. We have also proposed the bcc to hcp transformation path, which we investigated in iron [67] and in intermetallic compounds TiAl and NiAl [68]. Very recently, we have studied the tetragonal bcc-fcc transformation path in iron and have shown how these results may be used to predict the lattice constants and magnetic order of iron overlayers on various metallic substrates [69, 70]. This research is closely connected with the studies of iron stability performed in Refs. [71-76].

Another area of importance of the local stability of non-equilibrium phases and phase transformation paths is the structure of extended defects in solids. It was found in recent studies that atomic configurations in grain boundary (GB) regions, or at other interfaces, may contain certain metastable structures, different from the ground-state structures. For example, the 9R (α-Sm) structure was theoretically predicted and verified by high-resolution electron microscopy (HREM) at GBs in silver and copper [77, 78]. Similarly, the bcc structure was found at certain grain boundaries in copper [79]. We have shown [80] that the bcc Cu at grain boundaries is stabilized by external constraints exerted by the surrounding fcc grains and studied stabilization of higher-energy phases in pseudomorphic films [81].

Occurrence of such phases at interfaces is even more likely in more complex non-cubic alloys. For example, new structural features of TiAl, which crystallizes in tetragonal $L1_0$ structure, have been discovered recently. Abe et al. [82] found a B19-type hcp-based structure in a Ti-48at.%Al alloy quenched from the disordered phase, and Banerjee et al. [83] observed a series of structural transitions in the form of changes in the stacking sequence of the close-packed atomic planes in the Ti and Al layers in Ti/Al multilayered thin films.

Consequently, in order to explore adequately extended defects both in pure metals and alloys, in particular in intermetallics, detailed information about possible metastable structures, as well as lattice transformations connecting them, is needed. Armed with this knowledge one can predict whether an interface may be associated with a metastable structure and assess thus its stability and ability to transform to other structures (for example during deformation or due to changes in stoichiometry).

The purpose of the present paper, which is based on a recent presentation [62], is to study lattice configurations found in the course of tetragonal and trigonal displacive transformation (deformation) paths. These configurations are produced by large homogeneous distortions that transform the initial (ground-state) structure into new (higher-energy) structures with different symmetries. Such investigations are closely linked with theoretical strength and phase transformations and constitute a basis for future analyses of various configurations of extended defects in metallic materials. As specific examples, we study iron and the intermetallic compound Ni_3Al. Iron exists in both bcc and fcc modifications and has many magnetic phases, especially in thin films. Notably, fcc iron films exhibit a large variety of structural and magnetic properties that depend delicately on the thickness of the iron layer and preparation conditions [84]. Ni_3Al is the most important strengthening constituent of commercial nickel-based superalloys used extensively as structural materials for elevated temperatures applications. This phase is responsible for the high-temperature strength and creep resistance of the superalloys. Ni_3Al and a number of other intermetallic compounds with the $L1_2$ structure exhibit so-called anomalous yield behav-

ior, when their yield strength increases rather than decreases with increasing temperature. This behavior is not the result of a change in long-range order with temperature since the (Bragg) long-range parameter, S, is almost constant in Ni_3Al up to 1000 ^oC. There is now near-universal agreement that the anomaly results from the special properties of screw dislocation cores and the anisotropy in antiphase boundary energies; a review and comparison of various models are presented in Ref. [85]. Single crystals of Ni_3Al are ductile, but pure polycrystalline Ni_3Al is very brittle at room temperature because of intergranular fracture. Both iron and Ni_3Al exhibit magnetic ordering; therefore, we also study the changes of the magnetic state of these materials during deformation.

2. Displacive phase transformation paths

We consider two simple transformation paths connecting cubic structures. They are the bcc-fcc transformation path via tetragonal deformation corresponding to extension along the [001] axis (the usual Bain's path) and the trigonal deformation path that corresponds to uniaxial deformation along the [111] axis (Figs. 1 and 2).

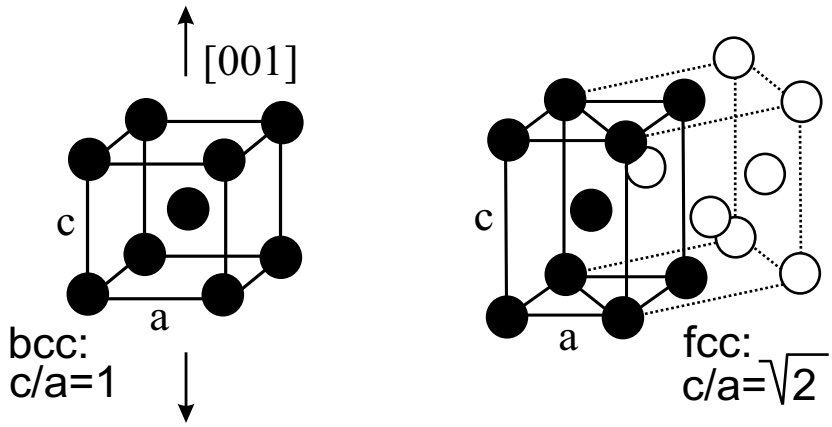

Figure 1: High-symmetry structures obtained along the tetragonal deformation path. The c and a are the length scales along the [001] and [100] directions, respectively. The original bcc cell is indicated by full circles and heavy solid lines.

In the case of tetragonal deformation path, we start with the bcc structure considered as a tetragonal one with the ratio $c/a = 1$, where c is measured along the [001] direction and a along a [100] direction. When c/a is varied, we arrive at body-centered tetragonal structures. There is one exception: for $c/a = \sqrt{2}$ the structure becomes fcc (Fig. 1).

Similarly, we may consider the bcc structure as trigonal with the ratio of $c/a = 1$, where c is measured along the [111] direction and a along a direction perpendicular to [111]. If $c/a \neq 1$, the structure becomes trigonal except for $c/a = 2$, when we attain the simple cubic (sc) structure, and $c/a = 4$, which again corresponds to the fcc structure (see Fig. 2).

When studying the behavior of the total energy along the deformation paths, one usually assumes that the atomic volume is constant. Then both deformation paths discussed above may be fully parameterized by the ratio c/a.

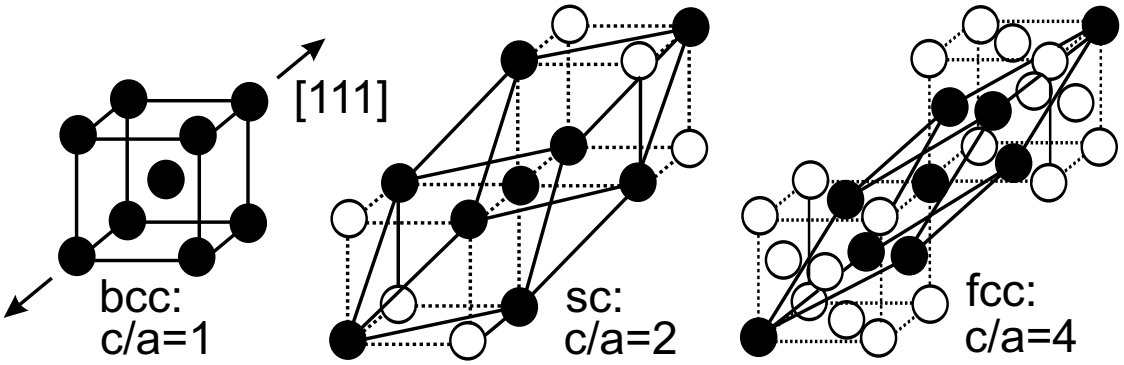

Figure 2: High-symmetry structures obtained along the trigonal deformation path. The c and a are the length scales along the [111] direction and along a direction perpendicular to [111], respectively.

Analogous deformation paths may be devised for intermetallic compounds with B2, $L1_2$ or $D0_3$ structures [18, 86]. In the $L1_2$ (Cu_3Au) structure, the atoms are at the fcc positions with the (002) planes occupied alternatively by Cu atoms and by Cu and Au atoms in the same ratio. We may consider this structure as tetragonal or trigonal with the ratio $c/a = 1$. Now, performing a tetragonal deformation, the cubic symmetry of the $L1_2$ configuration is lost and becomes tetragonal, even for $c/a = \sqrt{2}/2$, when atoms are at the bcc-like positions, but because we have two kinds of atoms, the structure does not attain the cubic symmetry. When we perform the trigonal deformation, the structure becomes trigonal except for the case of $c/a = 0.5$, when we encounter a simple-cubic-based structure that, indeed, has a cubic symmetry. For $c/a = 0.25$, the atoms adopt the bcc-like positions, but the symmetry of the structure remains trigonal. All these structures will be characterized in more details in a subsequent publication [86]. (Note different "normalization" of the ratio c/a for the $L1_2$ structure. Here we ascribed the value of $c/a = 1$ to the fcc-based configuration. Consequently, as it may be seen from Figs. 1 and 2, the bcc-based configuration, obtained by the tetragonal deformation, corresponds to $c/a = \sqrt{2}/2$, and the sc- and bcc-based structures, obtained by the trigonal deformation, correspond to $c/a = 0.5$ and $c/a = 0.25$, respectively.)

Craievich et al. [16] have shown that some energy extrema on constant-volume transformation paths are dictated by the symmetry. Namely, most of the structures encountered along the transformation paths between some higher-symmetry structures, say between bcc and fcc at the Bain's path, have a symmetry that is lower than cubic. At those points of the transformation path where the symmetry of the structure is higher, the derivative of the total energy with respect to the parameter describing the path must be zero. These are the so-called symmetry-dictated extrema. However, other extrema may occur that are not dictated by the symmetry and reflect properties of the specific material. The same is true for the transformation paths corresponding to uniaxial loading [20, 87]. Configurations corresponding to energy minima at the transformation paths represent stable or metastable structures and may mimic atomic arrangements that could be encountered when investigating thin films [20] and extended defects such as interfaces or dislocations [18, 68]. For iron and Ni_3Al, we will discuss these configurations below.

3. Tensile test simulation

To simulate a uniaxial tensile test, we start by determining the structure and total energy of the material in the ground state. Then, in the second step, we apply an elongation along the loading axis by a fixed amount ε that is equivalent to application of a certain tensile stress σ. For each value of ε, we minimize the total energy by relaxing the stresses $\sigma_{\perp 1}$ and $\sigma_{\perp 2}$ in the directions perpendicular to the loading axis. The stress σ is given by [88]

$$\sigma = \frac{c}{V}\frac{\partial E}{\partial c} = \frac{1}{Ac_0}\frac{\partial E}{\partial \varepsilon}, \tag{1}$$

where E is the total energy per repeat cell, V is the volume of the repeat cell, c is the dimension of the repeat cell in the direction of loading, A (equal to V/c ratio) is the area of the basis of the repeat cell in the plane perpendicular to the loading axis, and c_0 is the value of c in the undeformed state.

We are also interested in tensile strength at isotropic triaxial (hydrostatic) tension. In this case, we start again with the material in its ground-state structure, but the dimension of the crystal is gradually increased homogeneously in all directions. The hydrostatic stress σ is then calculated using the formula $\sigma = dE/dV$.

The inflexion point in the dependence of the total energy on elongation yields the maximum of the tensile stress; if any other instability (violation of some stability condition, soft phonon modes, magnetic spin arrangement etc.) does not occur prior to reaching the inflexion point, it also corresponds to the theoretical tensile strength, σ_{th}.

4. Methods of calculation

The atomic configurations corresponding to the deformed structures have usually a lower symmetry and, at the strength limit, they are very far from the ground state. Therefore, to get reliable structural energy differences, we must use a full-potential method for the calculations. Here we use the full-potential linearized augmented plane wave (FLAPW) code WIEN97 described in detail in Ref. [89]. The exchange-correlation energy is evaluated within the generalized-gradient approximation (GGA) [90]. This is important especially for iron, since the local density approximation does not render the ground state of iron correctly. The muffin-tin radius of iron atoms of 1.90 au is kept constant for all calculations. The number of $\boldsymbol{k}$-points in the whole Brillouin zone is equal to 6000 and the product of the muffin-tin radius and the maximum reciprocal space vector, $R_{MT}\ k_{max}$, is set to 10. The maximum l value for the waves inside the atomic spheres, l_{max}, and the largest reciprocal vector in the charge Fourier expansion, G_{max}, is equal to 12 and 15, respectively. In the case of Ni_3Al, the muffin-tin radii of both Ni and Al atoms are equal to 2.0 au, number of $\boldsymbol{k}$-points in the whole Brillouin zone is 4000, and the product $R_{MT}\ k_{max} = 8$. The values of l_{max} and G_{max} are 12 and 10, respectively.

5. Results and discussion

5.1. Iron

5.1.1. Total energies and magnetic states of tetragonally and trigonally deformed iron. We have calculated the total energy and magnetic moment of iron deformed along the tetragonal and trigonal paths at constant atomic volumes ranging from $V/V_{exp} = 0.84$ to $V/V_{exp} = 1.05$, where V_{exp} is the experimental equilibrium atomic volume of the ferromagnetic bcc iron corresponding to the lattice constant $a_{bcc} = 5.408$ au. As shown in Figs. 3 and 4, we include non-magnetic (NM), ferromagnetic (FM) and two antiferromagnetic states, namely the single-layer antiferromagnetic state (AFM1), in which the (001) or (111) planes have alternating magnetic moments ($\uparrow\downarrow\uparrow\downarrow\ldots$), and the double-layer antiferromagnetic state (AFMD), where the pairs of (001) or (111) planes have alternating magnetic moments ($\uparrow\uparrow\downarrow\downarrow\ldots$). The total energy of iron is plotted as a function of volume and the c/a ratio in Figs. 5 and 6. We show only those states the energies of which are the lowest for a given configuration. In Fig. 5, we can clearly see the "horseshoes" dividing the plane into the AFM1, AFMD and FM regions whereas the area of Fig. 6 is dominated by the FM states. The global minimum of energy is in the FM region at $c/a = 1$, $V/V_{exp} = 0.985$, which corresponds to the bcc structure. The calculated equilibrium volume is about 1.5 % lower than the experimental value, which may be considered as a very good agreement.

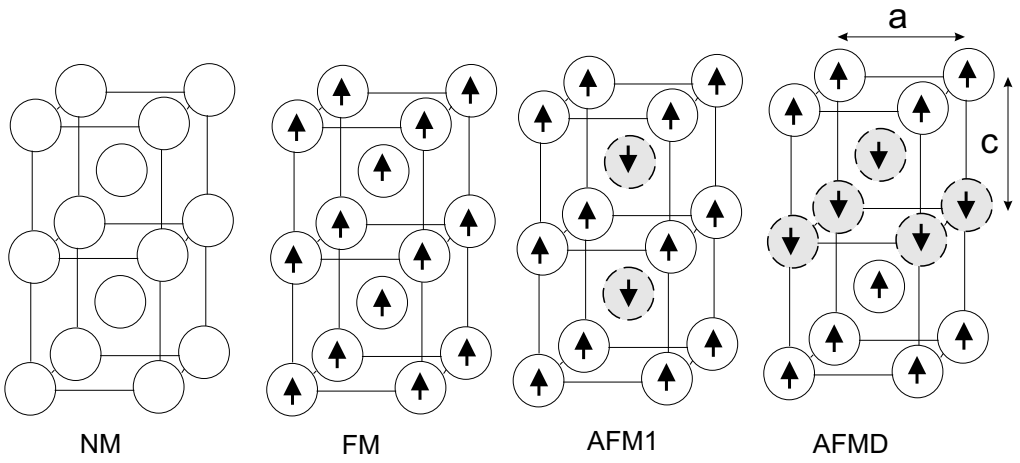

Figure 3: Non-magnetic (NM), ferromagnetic (FM), antiferromagnetic single-layer (AFM1) and antiferromagnetic double layer (AFMD) states of iron included in calculations of total energy profiles along tetragonal deformation paths.

The ground-state energy minimum is dictated by the symmetry. Any energy profile at the constant volume, obtained from Figs. 5 and 6, also exhibits the minimum at $c/a = 1$.

Let us discuss the tetragonal case first (Fig. 5). Apart from the large FM area, there are AFMD and AFM1 regions in the neighborhood of the fcc structure, which corresponds to the line $c/a = \sqrt{2}$. Note that the lattice symmetry of the fcc iron with the AFM1 and AFMD spin ordering is tetragonal and, therefore, we do not find any extremum of the total energy of these states (dictated by symmetry) at $c/a = \sqrt{2}$. In accordance with Ref. [72], we found that the fcc iron with the AFM1 or AFMD spin ordering is unstable with respect to the tetragonal deformation.

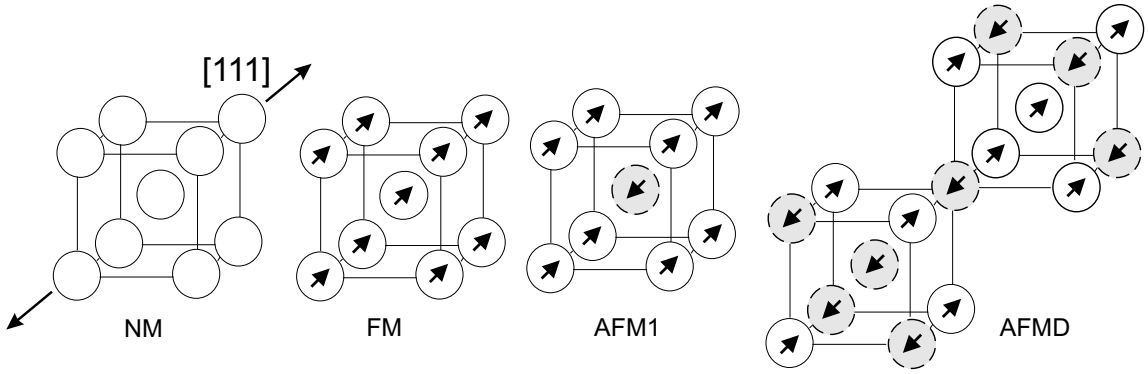

Figure 4: Non-magnetic (NM), ferromagnetic (FM), antiferromagnetic single-layer (AFM1) and antiferromagnetic double layer (AFMD) states of iron included in calculations of total energy profiles along trigonal deformation paths. (Note that these figures do not display all the (111) planes in the lattices shown).

A more detailed discussion of the tetragonal case is presented in Refs. [69, 70]. In those papers, we also showed how the contour plot presented in Fig. 5 may be used to predict the lattice parameters and magnetic states of iron overlayers at (001) substrates.

The AFMD structure with the tetragonal symmetry may be considered as a close approximation of the spin-spiral state with $\mathbf{q} = (2\pi/a)$ (0, 0, 0.6), found as the ground state of the fcc iron [91]. It will be the topic of future studies to ascertain how the non-collinearity of magnetic moments changes the borders between various magnetic phases in the (c/a, V/V_{exp}) plane. We surmise that the region of non-collinear magnetism will not be too different from the AFMD region shown in Fig. 5.

The AFM1 and AFMD states with the trigonal symmetry (Fig. 4) have mostly higher energy than the FM states and, consequently, they are nearly invisible in Fig. 6, except for the lower right corner. However, two regions of the FM states may be found in Fig. 6: FM(HS), the high-spin states (with magnetic moment higher than about 2 μ_B) and FM(LS), the low-spin states (with magnetic moment lower than about 1.2 μ_B). There is a sharp discontinuity in the magnetic moment at the border FM(HS)/FM(LS). Nonetheless, the total energy remains surprisingly smooth. The triangles in Fig. 6 denote local energy minima of fcc FM states and the square marks the point where the volume dependencies of the total energies of the fcc FM(HS) and FM(LS) states, displayed in Fig. 7, intersect. From Fig. 7 we see that the square represents a "sharp" saddle point in Fig. 6.

All total energy profiles at a constant volume $V > 0.955\ V_{exp}$ exhibit three symmetry-dictated extrema: a minimum at $c/a = 1$ (bcc structure), a maximum at $c/a = 2$ (sc structure) and a minimum at $c/a = 4$ (fcc structure). The reason is that both FM and NM structures exhibit a higher (cubic) symmetry at those values of c/a. The profile of the total energy at the constant volume $V = V_{exp}$, obtained from Fig. 6, is shown in Fig. 8. It is qualitatively similar to the total energy profiles of trigonally deformed Ta [92, 93] or Ir [18] and Cu [80] (the ground-state structure of Ir and Cu is fcc and, therefore the fcc minimum for those metals is lower than the bcc minimum).

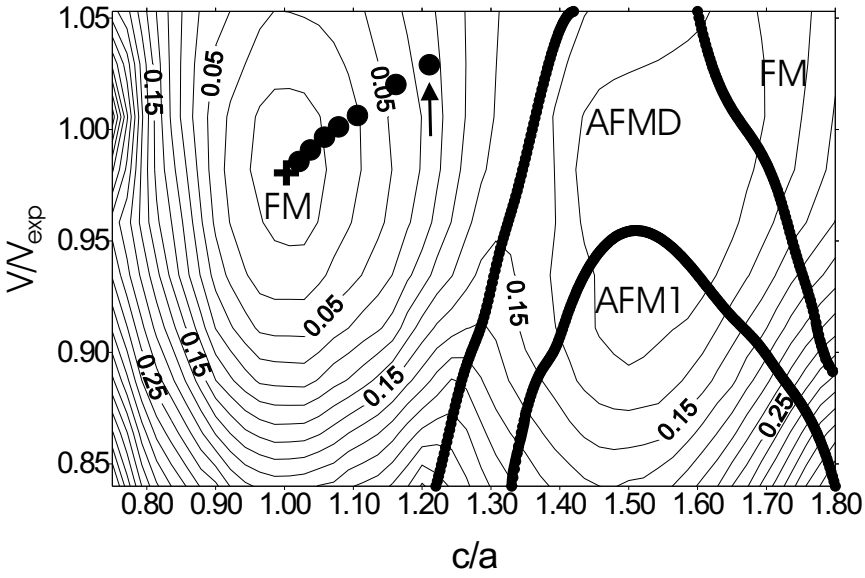

Figure 5: Total energy (per atom) of iron as a function of the tetragonal c/a ratio and volume relative to the energy of the FM bcc equilibrium state calculated within the GGA. Only states with the minimum energy are shown. The contour interval is equal to 20 meV. Thick lines show the FM/AFMD and AFMD/AFM1 phase boundaries. The cross corresponds to the global, symmetry-dictated minimum (ground state). The path representing the simulation of the tensile test for loading along the [001] direction is denoted by full circles; the highest circle marked by an arrow corresponds to the maximum stress obtained in the simulation of the tensile test.

5.1.2. Uniaxial and isotropic triaxial tensile tests. In accordance with methodology described in Sec. 3, we performed the simulation of a tensile test in iron for uniaxial loading along the [001] and [111] directions, respectively, as well as for isotropic triaxial loading corresponding to the negative hydrostatic pressure. The corresponding total energies as functions of relative elongation ε are displayed in Fig. 9(a). In case of the isotropic triaxial loading, ε corresponds to a relative extension of the bcc lattice parameter

It is seen from Fig. 9(a) that the total energy profiles have a parabolic, convex character in the neighborhood of the ferromagnetic (FM), symmetry-dictated, minimum that corresponds to the bcc structure (ground state). With increasing value of ε the curves reach (due to non-linear effects) their inflexion points (marked by vertical lines in Fig. 9(a)) and become concave. The inflexion point for [001] uniaxial loading occurs (most likely incidentally) for nearly the same elongation of $\varepsilon = 0.15$ as for the isotropic triaxial loading. In the case of the [001] tensile test, this elongation corresponds to the lattice parameter in the direction of loading equal to 6.20 au (accompanied by relaxation in [100] and [010] directions in which the lattice constant decreases to 5.12 au) and, in the case of isotropic triaxial strain, to the bcc structure with the lattice constant of 6.20 au.

The tensile stresses calculated according to formulas given in Sec. 3 are shown in Fig. 9(b). The inflexion points on the total energy profiles correspond to maximum stresses which the material may accommodate if its structure type does not change during the deformation. They are equal to $\sigma_{max}^{[001]} = 12.7$ GPa (this value was reported in our previous work [57] and is not very different

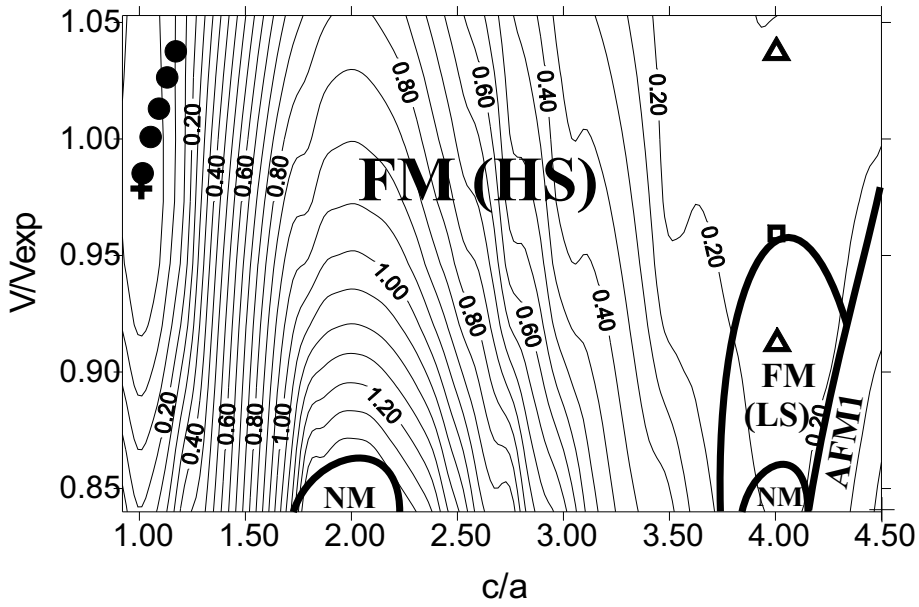

Figure 6: Total energy (per atom) of iron as a function of the trigonal c/a ratio and volume relative to the energy of the FM bcc equilibrium state, calculated within the GGA. Only states with the minimum energy are shown. The contour interval is equal to 50 meV. Thick lines show the FM(HS)/NM, FM(HS)/FM(LS), FM(LS)/NM and FM(LS)/AFM1 phase boundaries. The cross corresponds to the global symmetry-dictated minimum (ground state), the triangles show the local minima of the total energy of the fcc states in the FM(HS) and FM(LS) region at $V/V_{exp} = 1.037$ and 0.911, respectively. The square at $V/V_{exp} = 0.955$ denotes the crossing point of the dependencies of the total energy of the FM(HS) and FM(LS) fcc states on volume, presented in Fig. 7. As Fig. 7 shows, this square represents a "sharp" saddle point. The path representing simulation of the tensile test for loading along the [111] direction is denoted by full circles; the state corresponding to the maximum stress attained in the tensile test simulation ($V/V_{exp} = 1.114$, $c/a = 1.356$) lies outside the area of the figure.

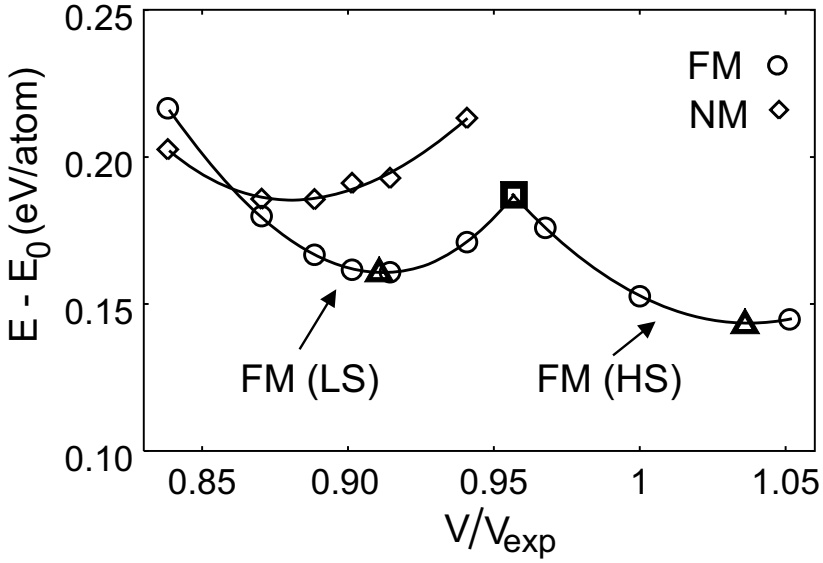

Figure 7: Total energies of the fcc FM and NM states of iron as functions of volume relative to the total energy of the FM bcc ground state. The triangles denote local energy minima (for their exact position see the description of Fig. 6), and the square corresponds to the intersection of the FM(HS) and FM(LS) curves.

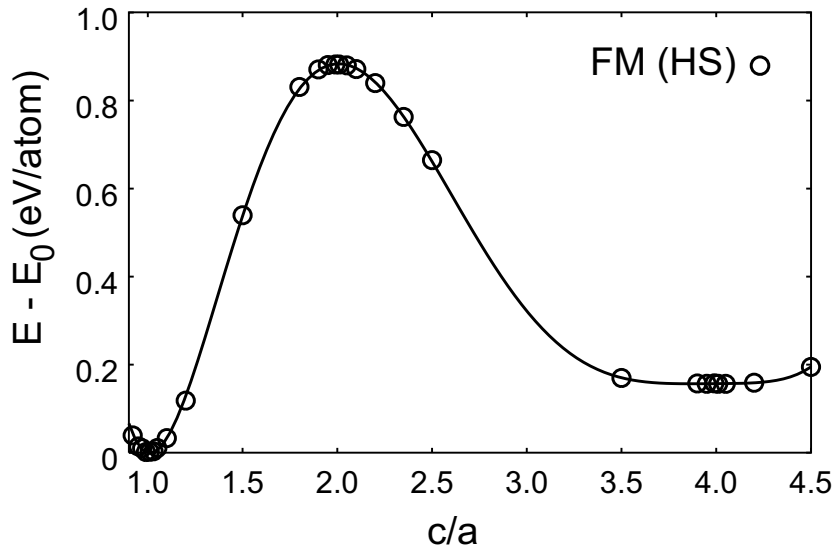

Figure 8: The profile of the total energy of trigonally deformed iron at $V/V_{exp} = 1$ (cf. with Fig. 6). All energy extrema (at $c/a = 1$, 2 and 4) are dictated by symmetry.

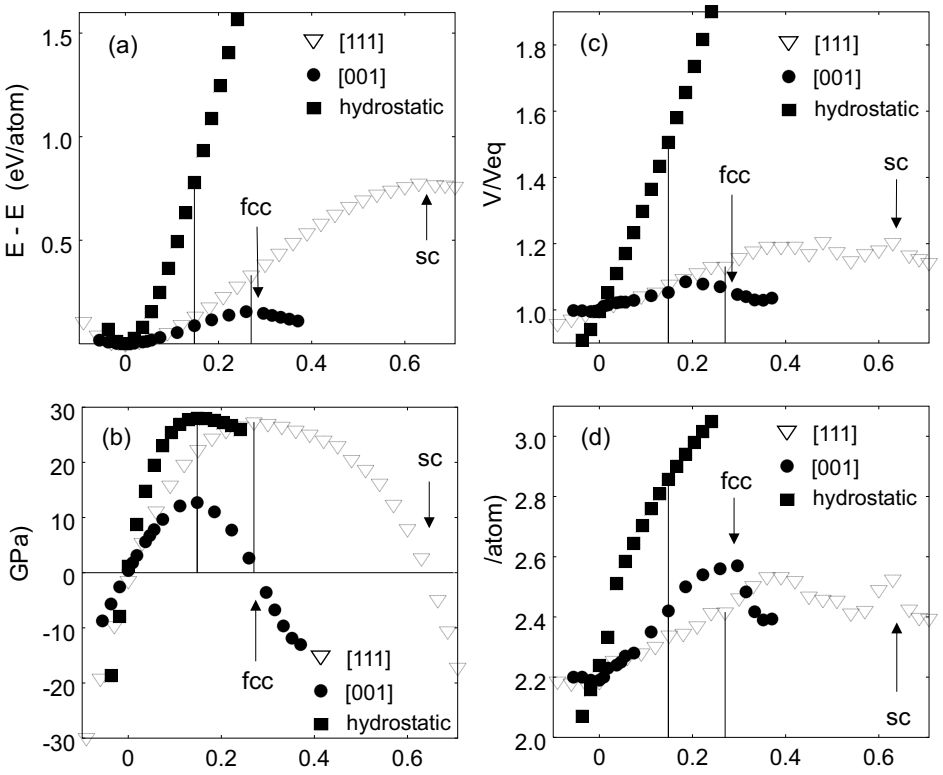

Figure 9: Total energy per atom measured with respect to the energy of the equilibrium state (a), stress (b), relative atomic volume ratio measured with respect to the equilibrium volume V_{eq} (c), and magnetic moment per atom μ (d) of FM iron loaded hydrostatically (full squares) and uniaxially along the [001] (full circles) and [111] (empty triangles) directions vs. elongation ε. The relative elongation ε reflects the changes of the lattice parameter a_{bcc} for isotropic triaxial loading and, in the case of uniaxial tensile tests, the increase/decrease of the crystal dimension in the directions of loading. The thin vertical lines mark the states exhibiting maximum stress (i.e. theoretical tensile strength). Incidentally, the maximum stresses for [001] uniaxial and isotropic triaxial (hydrostatic) loading are reached at nearly the same strain ε and, therefore, the corresponding vertical lines coincide.

from 14.2 GPa found in Ref. [58]), $\sigma_{max}^{[111]} = 27.3$ GPa and $\sigma_{max}^{[hydrostatic]} = 27.9$ GPa for uniaxial tensile test along the [001] and [111] direction and for isotropic triaxial (hydrostatic) loading, respectively. These values represent the theoretical tensile strengths provided other instabilities (soft phonon modes, etc.) do not come forth before reaching the inflexion point. In the case of iron with its large variety of magnetic phases, another instability may originate from transitions between those phases. However, as it is seen from Figs. 5 and 6, no such transition appears during tensile tests along [001] and [111] directions (all states involved up to the maximum stress lie in the FM region). A similar situation arises for isotropic triaxial deformation [54]. Other conditions of stability [88, 94] will be analyzed in a subsequent publication, but our preliminary calculations indicate that they will not be violated. It should be noted that the theoretical strength for loading in the [111] direction, equal to 27.3 GPa, is nearly the same as that obtained for isotropic triaxial loading, 27.9 GPa. At present, we do not have any plausible explanation of this fact.

In Fig. 9(a), it is seen that there are also other extrema of the total energy dictated by symmetry – maxima corresponding to the fcc and sc structures when simulating tensile tests with loading along the [001] and [111] directions, respectively. These extrema are denoted by arrows in Fig. 9(a). Their presence dictates that the corresponding dependence of the energy on elongation must bend, which imposes certain limitations on the maximum stress [22]. In the cases when there is no symmetry-dictated maximum (e.g. in the uniaxial tensile test along the [001] direction of NiAl with the B2 structure in the ground state [24]), the maximum stress is usually higher.

Since the structural energy difference E_{sc}–E_{bcc} is about five times higher than the difference E_{fcc}–E_{bcc} (755 meV/atom compared to 155 meV/atom), the E vs. ε curve for the [111] loading must rise much higher, albeit for larger strains, than that for the [001] loading (see Fig. 9(a)). Consequently, for the tensile test in the [111] direction the inflexion point occurs at a higher strain and for a higher stress than in the test with loading in the [001] direction. Thus, similarly as for W [22], a marked anisotropy of ideal tensile strengths for the [001] and [111] loading directions may be understood in terms of structural energy differences of nearby higher-symmetry structures found at the deformation path.

Relative changes of atomic volume and the dependences of the magnetic moment of FM iron per atom are shown as functions of elongation in Figs. 9(c) and 9(d), respectively. In the neighborhood of the ground state structure the atomic volume increases with increasing elongation but it exhibits a more complex behavior at larger deformations. For isotropic triaxial loading, the magnetic moment shows monotonous increase with increasing volume (in agreement with Herper et al. [95]) while in tensile tests it exhibits local extrema at points corresponding to both higher-symmetry structures (maxima for fcc and simple cubic) as well as at some other points along the paths. Let us note that the increase of the magnetic moment with deformation in the neighbourhood of the bcc ground state in case of uniaxial tensile tests is also connected with increasing volume (cf. Figs. 9(c) and (d)).

5.2. Intermetallic compound Ni_3Al

In contrast to iron, in the case of Ni_3Al we start with the fcc-based $L1_2$ structure and, therefore,

as mentioned in Sec. 2, we renormalize the ratio c/a by ascribing the value of $c/a = 1$ to the $L1_2$ structure. As a result, the c/a for the tetragonal path is by a factor of $\sqrt{2}$ smaller and for the trigonal path by a factor of 4 smaller than in the case of iron.

Using the GGA, the minimum of the total energy is obtained for the ferromagnetic state with the lattice constant equal to 3.561 Å (6.729 au) and magnetic moment of 0.80 μ_B per formula unit. The lattice constant agrees very well with the experimental value [96] of 3.568 Å (6.743 au) whereas the experimental magnetic moment, 0.23 μ_B per formula unit, is much lower. When including the spin-orbital coupling, Xu et al. [97] obtained a value of 0.46 μ_B per formula unit, which is closer to the experimental value. At present, we are verifying this conclusion.

Figure 10 shows the total energy of Ni_3Al as a function of c/a for the trigonal deformation at the experimental lattice volume. This dependence displays a symmetry-dictated minimum at $c/a = 1$ (the ground-state, $L1_2$ structure) and a symmetry-dictated maximum at $c/a = 0.5$ (a sc-based structure exhibiting cubic symmetry). A subsidiary minimum occurs at $c/a \approx 0.27$, which is not dictated by the symmetry. In the structure obtained for $c/a = 0.25$, the atoms are at the bcc-like positions, but the symmetry of this structure remains trigonal.

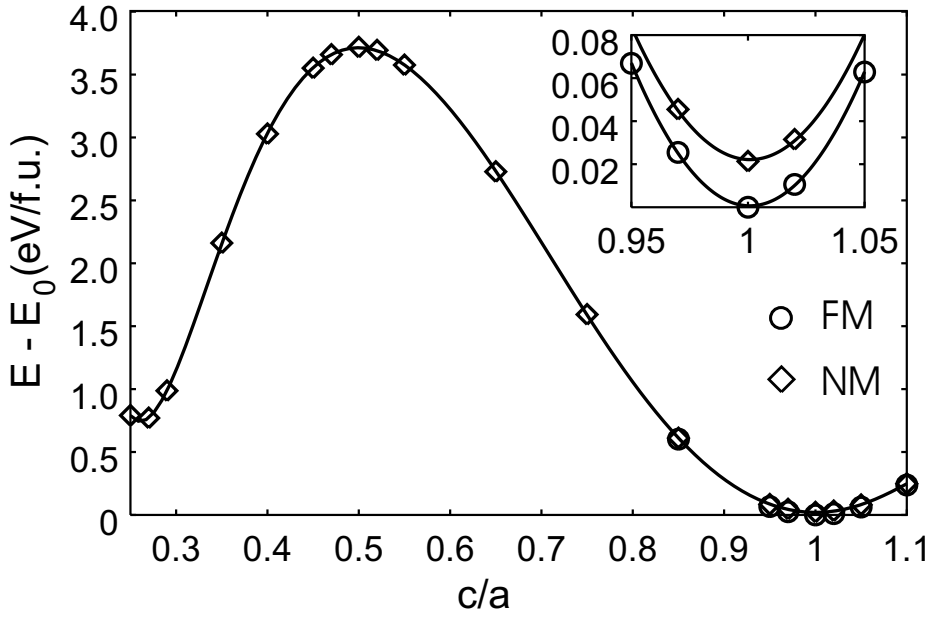

Figure 10: Total energy of Ni_3Al (per formula unit, f.u.) as a function of c/a for the trigonal deformation at the experimental lattice volume. The insert shows the details in the neighborhood of the ground state.

There is a very small energy difference between the FM and NM state of the $L1_2$ structure – only 21.3 meV/formula unit (see the insert in Fig. 10). This is consistent with the results of Xu et al. [97] (0.2-0.5 mRy/f.u.) and Min et al. [98] ($\sim$ 1 mRy/f.u.).

It is seen from Figs. 10 and 11 that the region of existence of FM state is limited. For $c/a \leq 0.75$, the magnetic moment is equal to zero (Fig. 11) and the compound is in a non-spin-polarized state.

Fig. 12 displays the total energy of Ni_3Al as a function of the volume and c/a for the trigonal

deformation. Again, we show only those states the energies of which are the lowest for a given configuration. The total energy profile presented in Fig. 10 is contained in Fig. 12 as a profile for $V/V_{exp} = 1$. A nearly vertical border divides the area of Fig. 12 into FM and NM regions. All energy profiles corresponding to a constant volume exhibit the symmetry-dictated maximum at $c/a = 0.5$. In the contour plot (Fig. 12), there is a saddle point for $c/a = 0.5$ and $V/V_{exp} \sim 1.2$ (outside the area of the figure). The minimum at $c/a \approx 0.27$, $V/V_{exp} \approx 1.01$ is not dictated by symmetry.

Fig. 13 shows the total energy of Ni_3Al as a function of the volume and c/a for the tetragonal deformation. Here NM regions extend to both sides of the FM ground state. However, there are no energy extrema and saddle points in those NM regions. It is interesting that the transition from the FM to NM state during both the trigonal and tetragonal deformation is essentially continuous, without any discontinuities in magnetic moment (see e.g. Fig. 11). Xu et al. [97] have shown that the energy gain in Ni_3Al associated with magnetism is about an order of magnitude smaller than that due to the structural differences. Our calculations show that the NM Ni_3Al in the $L1_2$ structure is stable with respect to tetragonal and trigonal deformations (the shear moduli C' and C_{44} are nearly the same for the NM and FM states). Therefore, magnetism does not appear to play an important role in the control of phase stability. This is in sharp contrast to iron, where the onset of ferromagnetism stabilizes the bcc structure and NM bcc states are not stable with respect to tetragonal deformation [69, 70].

Now, we can also simulate a tensile test in Ni_3Al to get theoretical tensile strengths for uniaxial loading along the [001] and [111] directions. These calculations are presently carried out.

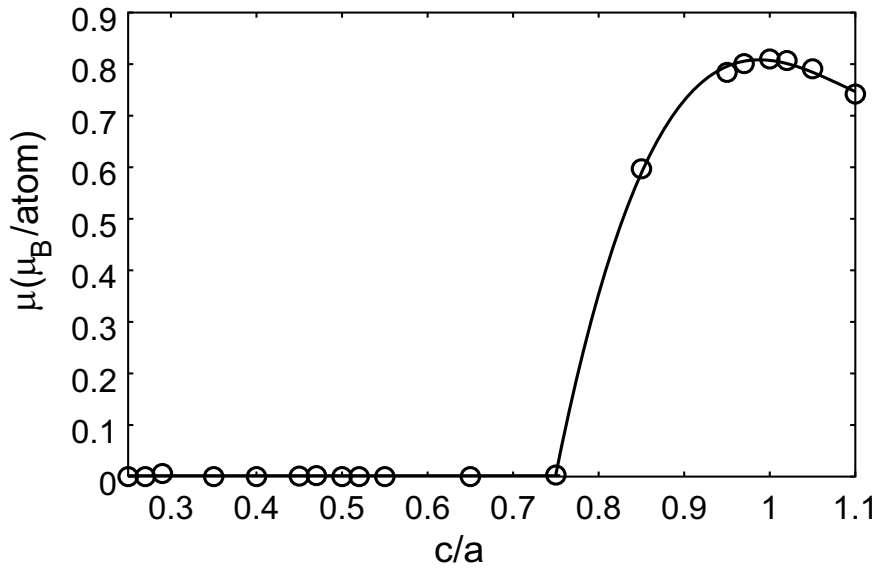

Figure 11: Magnetic moment of Ni_3Al as a function of c/a for the trigonal deformation at the experimental lattice volume.

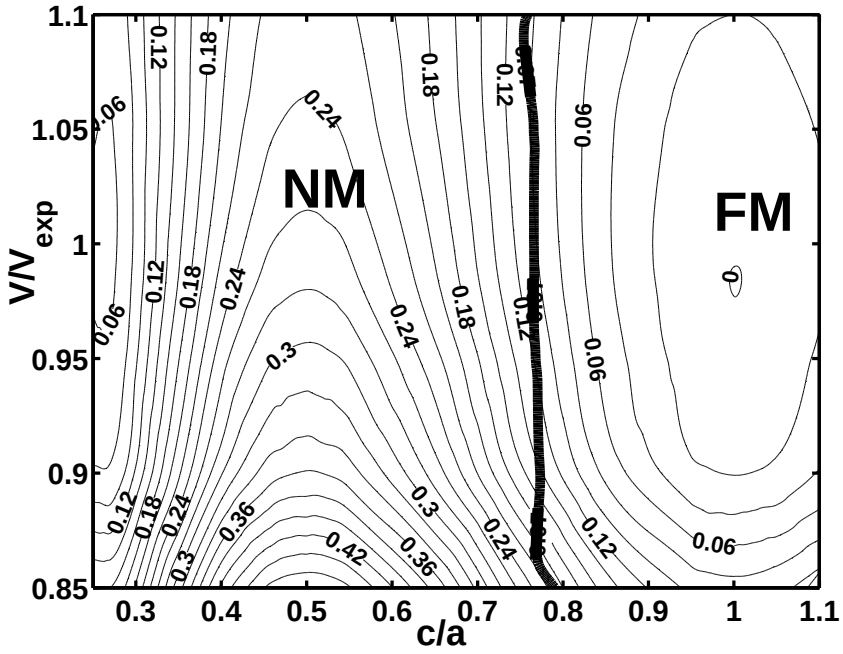

Figure 12: Total energy (per formula unit) of Ni_3Al as a function of volume and c/a ratio, characterizing the trigonal deformation, calculated within the GGA. The energy is measured relative to the energy of the equilibrium FM $L1_2$ state (the minimum at $c/a = 1$). Only states with the minimum energy are shown. The contour interval is 20 mRy. Thick line shows the NM/FM phase boundary. The ground-state minimum at $c/a = 1$ and the saddle point at $c/a = 0.5$ and $V/V_{exp} \sim 1.2$ (outside the figure area) are dictated by symmetry.

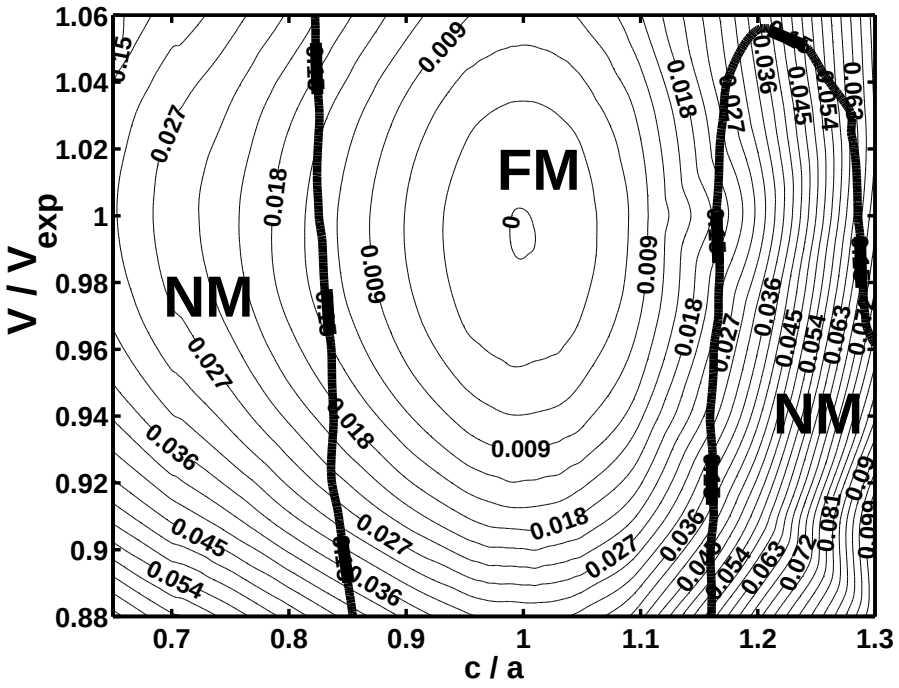

Figure 13: Total energy (per formula unit) of Ni_3Al as a function of volume and c/a ratio, characterizing the tetragonal deformation, calculated within the GGA. The energy is measured relative to the energy of the equilibrium FM $L1_2$ state (the minimum at $c/a = 1$). Only states with the minimum energy are shown. The contour interval is 3 mRy. Thick lines show the NM/FM phase boundaries. The only symmetry-dictated extremum is at $c/a = 1$.

6. Ab initio calculated values of theoretical tensile strength

For the sake of completeness, we summarize in the Table 1 all ab initio calculated values of the theoretical tensile strength (including relaxation in directions perpendicular to the loading axis and, if applicable, of internal structure parameters) that have been calculated until now. Most of them correspond to the inflexion point on the strain dependence of the total energy. Non-relaxed calculations are also included; th ecorresponding values are denoted by a dagger (†). As for the strength of W for [110] loading, the material probably breaks down due to some other instability before reaching the inflexion point and, therefore, the true theoretical tensile strength will be lower than that given in the Table. The situation is most likely the same in the case of Cu where the experimental ideal strengths are about an order of magnitude lower than the calculated ones [25, 99]. Semiempirical calculations [87] indeed suggest that, for the [001] direction, the tetragonal shear modulus becomes zero well before reaching the inflexion point. It may be expected that similar instabilities will occur for the [110] and [111] orientations. This will be the subject of further investigations.

7. Conclusions

We analyzed the energetics of iron and the intermetallic compound Ni_3Al subjected to tetragonal and trigonal deformation by means of full-potential ab initio electronic structure calculations and found borders between various phases with different spin polarizations. Whereas in iron the magnetic effects are vital for understanding the deformation behaviour and a variety of magnetic orderings occurs, it transpires that in Ni_3Al magnetism is not very important in phase stability considerations. The $L1_2$ ground state is ferromagnetic, but the energy difference between the FM and NM state is quite small, about 21 meV/formula unit. It is interesting that during tetragonal deformation, iron transforms to AFMD and AFM1 states (Fig. 5), whereas during trigonal deformation, it is mostly ferromagnetic (Fig. 6).

For iron, we analyzed uniaxial tensile tests and discussed the anisotropy of the theoretical tensile strength, namely 12.7 GPa for [001] and 27.3 GPa for the [111] direction of loading. This marked anisotropy may be understood in terms of the symmetry-dictated extrema that are present along the deformation paths. Also the isotropic triaxial (hydrostatic) tension was analyzed and theoretical tensile strength of iron for this mode of loading was found to be 27.9 GPa, very close to the value for uniaxial [111] loading.

It should be noted that the calculated dependence of the total energy on parameters of the transformation paths provides useful information when constructing semi-empirical interatomic potentials that may be used for computer simulation of atomic configurations of various extended defects for which the first-principles calculations are intractable. An example is bond-order potentials (BOPs) [100] for which we have shown recently how such first-principles results may be employed in their construction and testing [92, 101].

Stability of higher-energy structures is also an important issue in the theoretical basis of the CALPHAD (CALculation of PHAse Diagrams) method [102]. Grimvall [103, 104] concludes that when either the bcc or fcc structure of a metal is dynamically unstable, i.e. unstable, for example,

material	structure	direction	σ_{th} (GPa)	reference
Fe	A2	[001]	12.7	[57, 59]
		[001]	14.2	[58]
		[111]	27.3	[59]
W	A2	[001]	28.9	[22]
		[001]	29.5	[32]
		[111]	40.1	[22]
		[110]	54.3	[22]
Al	A1	[001]	12.1	[26]
		[111]	11.05	[26]
		[111]	11†	[27, 28]
Cu	A1	[001]	55†,32†	[13]
		[001]	33	[25]
		[110]	31	[25]
		[111]	29	[25]
diamond	A4	[111]	90	[35]
		[111]	95	[36]
		[001]	225	[35]
		[110]	130	[35]
Si	A4	[111]	22	[36]
Ge	A4	[111]	14	[36]
Nb	A2	[001]	13.1	[37]
Mo	A2	[001]	28.8	[37]
TiC	B1	[001]	44	[21]
NiAl	B2	[001]	46	[24, 25]
		[111]	25	[24, 25]
β-SiC	B3 (3C)	[001]	101	[34]
		[111]	50.8	[34]
AlN	B4	[0001]	50†	[27, 28]
$MoSi_2$	$C11_b$	[001]	37	[55, 56]
WSi_2	$C11_b$	[001]	38	[55, 56]
β-Si_3N_4	$P6_3/m$	[100]	72.2†	[38]
		[100]	57	[40]
		[001]	75.0†	[38]
		[001]	55	[40]
c-Si_3N_4	$Fd\bar{3}m$	[001]	45	[39]

Table 1: Theoretical tensile strengths σ_{th} calculated ab initio. The dagger means that the perpendicular dimensions of the sample were not relaxed during the calculations (no Poisson contraction allowed).

with respect to the tetragonal or trigonal deformation, then there are large discrepancies between the semiempirical enthalpy differences H_{bcc}-H_{fcc} obtained from the CALPHAD method and ab initio results. However, as we can see from Refs. [16, 18, 81], this is the case in most transition metals. In ab initio calculations, the dynamical instability is suppressed since we impose a rigid lattice (in reality, this might be stabilized by some external constraints), and the energy and enthalpy of such structure have well defined physical meaning. However, it appears that it is not certain how such values may be compared with those obtained from semiempirical CALPHAD method.

8. Acknowledgements

This research was supported by the Grant Agency of the Academy of Sciences of the Czech Republic (Project No. IAA1041302), by the Grant Agency of the Czech Republic (Project No. 202/03/1351), by the Research Project Z2041904 of the Academy of Sciences of the Czech Republic, and by the U.S. Department of Energy, Basic Energy Sciences (Grant No. DE-FG02-98ER45702). A part of this study has been performed in the framework of the COST Project No. OC 523.90. The use of the computer facilities at the MetaCenter of the Masaryk University, Brno, and at the Boston University Scientific Computing and Visualization Center is acknowledged.

9. References

[1] S. S. Brenner, J. Appl. Phys. **27**, 1484 (1956).
[2] S. S. Brenner, J. Appl. Phys. **28**, 1023 (1957).
[3] R. V. Coleman, B. Price and N. Cabrera, J. Appl. Phys. **28**, 1360 (1957).
[4] G. L. Pearson, W. T. Read Jr., and W. L. Feldmann, Acta Met. **5**, 181 (1957).
[5] E. M. Nadgorny, Sov. Phys. Uspekhi **5**, 462 (1962).
[6] R. P. Vinci and J. J. Vlassak, Ann. Rev. Mater. Sci. **26**, 431 (1996).
[7] D. F. Bahr, D. E. Kramer, and W. W. Gerberich, Acta Mater. **46**, 3605 (1998).
[8] A. Gouldstone, H. J. Koh, K. Y. Zeng, A. E. Giannakopoulos, and S. Suresh, Acta Mater. **48**, 2277 (2000).
[9] C. L. Woodcock and D. F. Bahr, Scripta Mater. **43**, 783 (2000).
[10] O. R. delaFuente, J. A. Zimmerman, M. A. Gonzalez, J. delaFiguera, J. C. Hamilton, W. W. Pai, and J. M. Rojo, Phys. Rev. Lett. **88**, 036101 (2002).
[11] F. Milstein and S. Chantasiriwan, Phys. Rev. B **58,** 6006 (1998).
[12] P. Šandera and J. Pokluda, Scripta Metall. Mater. **29**, 1445 (1993).
[13] E. Esposito, A.E. Carlsson, D.D. Ling, H. Ehrenreich, and C.D. Gelatt, Jr., Phil. Mag. **41**, 251 (1980).
[14] A.T. Paxton, P. Gumbsch, and M. Methfessel, Phil. Mag. Lett. **63**, 267 (1991).
[15] W. Xu, and J.A. Moriarty, Phys. Rev. B **54**, 6941 (1996).
[16] P.J. Craievich, M. Weinert, J.M. Sanchez, and R.E. Watson, Phys. Rev. Lett. **72**, 3076 (1994).

[17] L. Vitos, J. Kollár, and H.L. Skriver, in Stability of Materials, eds. A. Gonis, P.E.A. Turchi, and J. Kudrnovský, Plenum Press, New York-London, 1996, p. 393.
[18] M. Šob, L.G. Wang, and V. Vitek, Comp. Mat. Sci. **8**, 100 (1997).
[19] P.J. Craievich, J.M. Sanchez, R.E. Watson, and M. Weinert, Phys. Rev. B **55**, 787 (1997).
[20] P. Alippi, P.M. Marcus, and M. Scheffler, Phys. Rev. Lett. **78**, 3892 (1997).
[21] D.L. Price, B.R. Cooper, and J.M. Wills, Phys. Rev. B **46**, 11368 (1992).
[22] M. Šob, L.G. Wang, and V. Vitek, Mat.Sci. Eng. A **234-236**, 1075 (1997).
[23] I.M. Mikhailovskii, I. Ya. Poltinin, and L.I. Fedorova, Fizika Tverdogo Tela **23** 1291 (1981) (English translation in Sov. Phys. Solid State **23** 757 (1981)).
[24] M. Šob, L.G. Wang, and V. Vitek, Phil. Mag. B **78**, 653 (1998).
[25] M. Šob, L.G. Wang, V. Vitek, Kovové materiály (Metallic Materials) **36**, 145 (1998).
[26] W. Li and T. Wang, J. Phys.: Condens. Matter **10**, 9889 (1998).
[27] H. Kitagawa and S. Ogata, Key Engineering Materials **161-163**, 443 (1999)
[28] S. Ogata and H. Kitagawa, Comp. Mat. Sci. **15**, 435 (1999).
[29] D. Roundy, C.R. Krenn, M.L. Cohen, and J.W. Morris, Jr., Phys. Rev. Lett. **82**, 2713 (1999).
[30] C.R. Krenn, D. Roundy, J.W. Morris Jr., and M.L. Cohen, Mat. Sci. Eng. A **317**, 44 (2001).
[31] C.R. Krenn, D. Roundy, J.W. Morris Jr., and M.L. Cohen, Mat. Sci. Eng. A **319-321**, 111 (2001).
[32] D. Roundy, C.R. Krenn, M.L. Cohen, and J.W. Morris, Jr., Phil. Mag. A **81**, 1725 (2001).
[33] J.W. Morris, Jr. and C.R. Krenn, Phil. Mag. A **80**, 2827 (2000).
[34] W. Li and T. Wang, Phys. Rev. B **59**, 3993 (1999).
[35] R.H. Telling, C.J. Pickard, M.C. Payne, and J.E. Field, Phys. Rev. Lett. **84**, 5160 (2000).
[36] D. Roundy and M.L. Cohen, Phys. Rev. B **64**, 212103 (2001).
[37] W. Luo, D. Roundy, M.L. Cohen, and J.W. Morris, Jr., Phys. Rev. B **66**, 094110 (2002).
[38] S. Ogata, N. Hirosaki, C. Kocer, and H. Kitagawa, Phys. Rev. B **64**, 172102 (2001).
[39] C. Kocer, N. Hirosaki, and S. Ogata, Phys. Rev. B **67**, 035210 (2003).
[40] S. Ogata, N. Hirosaki, C. Kocer, and Y. Shibutani, J. Mater. Res. **18**, 1168 (2003).
[41] S.-H. Jhi, S.G. Louie, M.L. Cohen, and J.W. Morris, Jr., Phys. Rev. Lett. **87**, 075503 (2001).
[42] Y. Umeno and T. Kitamura, Mat. Sci. Eng. B **88**, 79 (2002).
[43] S. Ogata, J. Li, and S. Yip, Science **298**, 807 (2002).
[44] G. Galli, F. Gygi, and A. Catellani, Phys. Rev. Lett. **82**, 3476 (1999).
[45] F.J. Ribeiro, D.J. Roundy, and M.L. Cohen, Phys. Rev. B **65**, 153401 (2002).
[46] M. Kohyama, Mat Sci. Forum **294-296**, 657 (1999).
[47] M. Kohyama, Phys. Rev. B **65**, 184107 (2002).
[48] I.G. Batirev, A. Alavi, M.W. Finnis, and T. Deutsch, Phys. Rev. Lett. **82**, 1510 (1999).
[49] P. Šandera, J. Pokluda, L.G. Wang, and M. Šob, Mat. Sci. Eng. A **234-236**, 370 (1997).
[50] Y. Song, R. Yang, D. Li, W.T. Wu, and Z.X. Guo, Phys. Rev. B **59**, 14220 (1999).
[51] M. Černý, P. Šandera, and J. Pokluda, Czech. J. Phys. **49**, 1495 (1999).
[52] Y. Song, R.Yang, D. Li, and Z.X. Guo, Phil. Mag. A **81**, 321 (2001).

[53] Y. Song, Z.X. Guo, and R. Yang, Phil. Mag. A **82**, 1345 (2002).
[54] M. Černý, J. Pokluda, P. Šandera, M. Friák, and M. Šob, Phys. Rev. B **67**, 035116 (2003).
[55] M. Friák, M. Šob, and V. Vitek, in: High-Temperature Ordered Intermetallic Alloys IX, eds. J.H. Schneibel, K.J. Hemker, R.D. Noebe, S. Hanada, G. Sauthoff, MRS Symp. Proc. vol. **646**, Materials Research Society, Warrendale, PA, 2001, paper N4.8.
[56] M. Friák, M. Šob, and V. Vitek, Phys. Rev. B (2003), submitted.
[57] M. Friák, M. Šob, and V. Vitek, Proc. Int. Conf. JUNIORMAT'01, Faculty of Mechanical Engineering, Brno University of Technology, Brno, 2001, p. 117.
[58] D.M. Clatterbuck, D.C. Chrzan, and J.W. Morris, Jr., Phil. Mag. Lett. **82**, 141 (2002).
[59] M. Friák, M. Šob, and V. Vitek, Phil. Mag. (2003), accepted.
[60] M. Šob, L.G. Wang, M. Friák and V. Vitek, in Computational Modeling of Materials, Minerals, and Metals Processing, eds. M. Cross, J.W. Evans, and C. Bailey, The Minerals, Metals & Materials Society, Warrendale, PA, 2001, pp. 715-724.
[61] J.W. Morris, Jr., C.R. Krenn, D. Roundy, and M.L. Cohen, in Phase Transformations and Evolution in Materials, ed. P.E.A. Turchi and A. Gonis, The Minerals, Metals & Materials Society, Warrendale, PA, 2000, pp. 187-207.
[62] M. Šob, M. Friák, D. Legut, and V. Vitek, in Proc. 3rd Int. Alloy Conf.: An Interdisciplinary Approach to the Science of Alloys in Metals, Minerals and Other Materials Systems, eds. P.E.A. Turchi and A. Gonis, Estoril/Cascais, Portugal, June 30-July 5, 2002, to be published.
[63] J. Pokluda and P. Šandera, in METAL 2000 (Proc. 9^{th} Int. Metallurgical Conf., Ostrava, Czech Republic, May 16-18, 2000), ed. T. Prnka, Tanger, Ostrava, 2000.
[64] J.A. Moriarty, Phys. Lett. A **131**, 41 (1988).
[65] S. Fox and H.J.F. Jansen, Phys. Rev. B **53**, 5119 (1996).
[66] M.J. Mehl and D.A. Papaconstantopoulos, Phys. Rev. B **54**, 4519 (1996).
[67] M. Šob, M. Friák, L.G. Wang, and V. Vitek, in Multiscale Modelling of Materials, eds. V.V. Bulatov, T. Diaz de la Rubia, R. Phillips, E. Kaxiras, N. Ghoniem, Mater. Res. Soc. Symp. Proc. vol. **538**, Materials Reseach Society, Warrendale, PA, 1999, pp. 523-527.
[68] V. Paidar, L.G. Wang, Šob, V. Vitek, Modelling Simul. Mater. Sci. **7**, 369 (1999).
[69] M. Friák, M. Šob, and V. Vitek, Phys. Rev. B **63**, 052405 (2001).
[70] M. Friák, M. Šob, and V. Vitek, in Electron Correlations and Material Properties 2, eds. A. Gonis, N. Kioussis, and M. Ciftan, Kluwer Academic/Plenum Publishers, New York, 2003, pp. 399-415.
[71] D. Spišák and J. Hafner, Phys. Rev. B **61**, 16129 (2000).
[72] S.L. Qiu, P.M. Marcus, and H.Ma, J. Appl. Phys. **87**, 5932 (2000).
[73] S.L. Qiu, P.M. Marcus, and H.Ma, Phys. Rev. B **64**, 104431 (2001).
[74] D. Spišák and J. Hafner, Phys. Rev. Lett. **88**, 056101 (2002).
[75] D. Spišák and J. Hafner, Phys. Rev. B **65**, 235405 (2002).
[76] H. Ma, S.L. Qiu, and P.M. Marcus, Phys. Rev. B **66**, 024113 (2002).
[77] F. Ernst, M.W. Finnis, D. Hofmann, T. Muschik, U. Schönberger, and U. Wolf, Phys. Rev. Lett. **69**, 620 (1992).
[78] D. Hofmann and M.W. Finnis, Acta Metall. Mater. **42**, 3555 (1994).

[79] C. Schmidt, F. Ernst, M.W. Finnis, and V. Vitek, Phys. Rev. Lett. **75**, 2160 (1995).
[80] L.G. Wang and M. Šob, Phys. Rev. B **60**, 844 (1999).
[81] L.G. Wang, M. Šob, and Z. Zhang, J. Phys. Chem. Solids **64**, 863 (2003).
[82] E. Abe, T. Kumagai, and M. Nakamura, Intermetallics **4**, 327 (1996).
[83] R. Banerjee, R. Ahuja, and H.L. Fraser, Phys. Rev. Lett. **76**, 3778 (1996).
[84] H. Jenniches, J. Shen,, Ch.V. Mohan, S.S. Manoran, J. Barthel, P. Ohresser, M. Klaua, and J. Kirschner, Phys. Rev. B **59**, 1196 (1999).
[85] V. Vitek, D.P. Pope, J, Bassani, in Dislocations in Solids **10** (Plasticity of Gamma Alloys), ed. F.R.N. Nabarro and M.S. Duesberry, Elsevier Science Publishers, Amsterdam, 1996, p. 135.
[86] D. Legut, M. Friák, L.G. Wang, and M. Šob, to be published.
[87] F. Milstein and B. Farber, Phys. Rev. Lett. **44**, 277 (1980).
[88] D.J. Rasky and F. Milstein, Phys. Rev. B **33**, 2765 (1986).
[89] P. Blaha, K. Schwarz, J. Luitz, WIEN97, Technical University of Vienna 1997 -improved and updated Unix version of the original copyrighted WIEN-code, which was published by P. Blaha, K. Schwarz, P. Sorantin, S. B. Trickey, in: Comput. Phys. Commun. **59**, 399 (1990).
[90] J. P. Perdew, S. Burke, M. Ernzerhof, Phys. Rev. Lett. **77**, 3865 (1996).
[91] L.M. Sandratskii, Adv. Phys. **47**, 91 (1998).
[92] M. Mrověc, V. Vitek, D. Nguyen-Manh, D.G. Pettifor, L.G. Wang, and M. Šob, in Multiscale Modeling of Materials, eds. V.V. Bulatov, T. Diaz de Rubia, R. Phillips, E. Kaxiras, and N. Ghoniem, MRS Symposium Proc. vol. **538**, Materials Research Society, Warrendale, PA, 1999, pp. 529-534.
[93] M. Šob, M. Friák, L.G. Wang, and V. Vitek, Key Eng. Materials **227**, 261 (2002).
[94] J. Wang, J. Li, S. Yip, S. Phillpot, and D. Wolf, Phys. Rev. B **52**, 12627 (1995).
[95] H. C. Herper, E. Hoffmann, P. Entel, Phys. Rev. B **60**, 3839 (1999).
[96] F.R. de Boer, C.J. Schinkel, J. Biesterbos, and S. Proost, J. Appl. Phys. **40**, 1049 (1969).
[97] J. Xu, B.I. Min, A.J. Freeman, and T. Oguchi, Phys. Rev. B **41**, 5010 (1990).
[98] B.I. Min, A.J. Freeman, and H.J.F. Jansen, Phys. Rev. B **37**, 6757 (1988).
[99] H. Kobayashi and I. Hiki, Phys. Rev. B **7**, 594 (1973).
[100] D.G. Pettifor, Bonding and Structure of Molecules and Solids, Oxford University Press, Oxford, 1995.
[101] M. Mrověc, V. Vitek, D. Nguyen-Manh, D.G. Pettifor, L.G. Wang, and M. Šob, in Multiscale Phenomena in Materials - Experiment and Modeling, eds. D.H. Lassila, I.M. Robertson, R. Phillips, and B. Devincre, MRS Symp. Proc. vol. **578**, Materials Research Society, Warrendale, PA, 2000, pp. 199-204.
[102] N. Saunders and P. Miodownik, CALPHAD (Calculation of Phase Diagrams): A Comprehensive Guide, Pergamon Materials Series vol. **1**, ed. R.W. Cahn, Elsevier Science Publishers, Oxford-New York-Tokyo, 1998.
[103] G. Grimvall, Ber. Bunsenges. Phys. Chem. **102**, 1083 (1998).
[104] G. Grimvall, in Proc. 3rd Int. Alloy Conf.: An Interdisciplinary Approach to the Science of Alloys in Metals, Minerals and Other Materials Systems, eds. P.E.A. Turchi and A.

Gonis, Estoril/Cascais, Portugal, June 30-July 5, 2002, to be published.